JOURNAL OF AIRCRAFT
Vol. 39, No. 6, November–December 2002

Transition Measurements on the Natural Laminar Flow Wing at Mach 2

Hiroki Sugiura,* Kenji Yoshida,† Naoko Tokugawa,* Shohei Takagi,‡ and Akira Nishizawa§
National Aerospace Laboratory, Chofu, Tokyo 182-8522, Japan

Transition characteristics of a supersonic natural laminar flow wing with a sweep angle of more than 60 deg were measured using hot-film sensors and an infrared camera at Mach 2. The pressure falls very rapidly in the vicinity of the leading edge of the wing, such that crossflow instabilities are reduced. The flow slightly accelerates downstream such that streamwise instabilities are stabilized. Tests were conducted in two wind tunnels to estimate the transition location in flight: a quiet tunnel with a low Reynolds number and a moderately quiet tunnel with variable Reynolds number. As a result, the natural laminar flow effect of the wing was confirmed. The unit Reynolds number had no effect on the transition Reynolds number of the wing. The transition Reynolds number was 8×10^5 at the design angle of attack at Mach 2, but there is room for further investigation.

Nomenclature

C_P	=	pressure coefficient
$C_{P\,\mathrm{rms}}$	=	static pressure fluctuation normalized by dynamic pressure
c	=	wing chord length
h	=	roughness height
k	=	average roughness height
M	=	Mach number
P	=	pressure
Re	=	Reynolds number
s	=	half-span length
U	=	velocity along streamline
x	=	distance along wing chord
y	=	distance in spanwise direction
α	=	angle of attack, deg
δ	=	boundary-layer thickness
μ	=	viscosity coefficient
ρ	=	density
Ψ	=	angle between propagation direction of wave disturbance and outer streamline

Subscripts

k	=	at roughness height
max	=	maximum amplified disturbance
rms	=	root-mean-square average
tr	=	transition point
unit	=	unit
w	=	at wall
x	=	distance along wing chord
0	=	freestream stagnation conditions
02	=	isentropic stagnation conditions

Presented as Paper 2001-2782 at the 31st Fluid Dynamics Conference, Anaheim, CA, 11–14 June 2001; received 5 October 2001; accepted for publication 16 April 2002.

*Researcher, Transition and Turbulence Research Group, Fluid Science Research Center. Member AIAA.

†Leader, Aerodynamic Design Group, Next Generation Supersonic Transport Project Center. Member AIAA.

‡Leader, Transition and Turbulence Research Group, Fluid Science Research Center. Senior Member AIAA.

§Researcher, Transition and Turbulence Research Group, Fluid Science Research Center.

Introduction

FRICTION drag makes up more than one-third of the drag of next-generation supersonic transports (SST), and its reduction by delaying transition is very effective for improving the lift-to-drag ratio. An appropriate pressure distribution delays transition on a two-dimensional wing; this is called natural laminar flow (NLF) control because this is a passive boundary-layer control technique and requires no active system such as suction or cooling. Shaping the highly swept wing of SST is much more difficult because a compromise must be found between two opposing effects. Close to the leading edge, a favorable pressure gradient stabilizes streamwise instabilities (Tollmien–Schlichting waves), but it generates crossflow velocity components that amplify crossflow instability. An adverse pressure gradient reduces crossflow instability, but streamwise disturbances start to grow rapidly.

An NLF wing was designed at the National Aerospace Laboratory, Japan, on a nonpowered experimental airplane with optimal pressure drag at supersonic speeds.[1] As shown in Fig. 1, the pressure decreases very rapidly in the leading-edge region of the wing such that the development of crossflow velocity components that amplify crossflow instability is minimized. Downstream of the leading-edge region, the flow accelerates slightly such that streamwise instabilities are stabilized.

A significant amount of flight research[2–4] has been conducted on NLF control applied to various configurations: F-111/TACT (wing sweep angles of up to 26 deg), F-14 (up to 35 deg), Boeing 757 (21 deg), and Dassault Falcon 50 (35 deg). All of them have sweep angles of less than 40 deg. The present wing is the first NLF wing with a sweepback angle of more than 60 deg. (Sweep angles of the inner and outer parts of the wing are 66 and 61.2 deg, respectively.) For the purpose of validating a NLF wing with a sweepback angle of more than 60 deg, transition on the wing was measured in two supersonic wind tunnels. This report concerns transition measurement of the wing and an attempt to evaluate the NLF effect under an in-flight condition.

Procedure

Testing Facilities

To simulate boundary-layer transition on supersonic aircraft in ground facilities, a quiet low-turbulence environment with high Reynolds numbers is required. The freestream turbulence level in flight is extremely low. It is usually characterized by a single parameter, the static pressure fluctuation normalized by dynamic pressure $C_{P\,\mathrm{rms}}$; $C_{P\,\mathrm{rms}}$ varying from 0.03 to 0.08% is reported in flight.[5] Because there are very few supersonic wind tunnels that realize this condition at high Reynolds numbers,[6] transition locations are quite different in flight and in wind tunnels.[5] Hence, transition

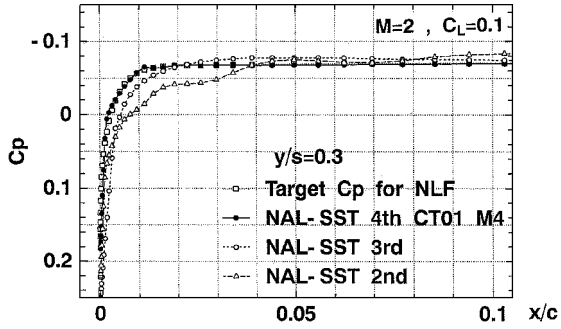

Fig. 1 Pressure distributions on the natural laminar flow wing at the design point.

measurements were conducted in two types of facilities to evaluate the transition locations in flight: a quiet tunnel with low Reynolds number and a moderately quiet tunnel with a wide range of Reynolds numbers. We used an in-draft supersonic tunnel from Fuji Heavy Industries, Ltd. (FHI tunnel) as the former and the ONERA continuous supersonic tunnel (S2MA) as the latter. In-draft tunnels have pressure control valves downstream of the test section. They are very quiet compared to other tunnels that have the test section downstream of disturbance sources such as pressure control valves and blowers.[7] The $C_{P\,\mathrm{rms}}$ of 0.05% has been reported in the FHI tunnel[8]; its test section is 0.61 m^2 in both length and width. The total pressure in S2MA ranges from 20 to 250 kPa; therefore, a wide range of Reynolds numbers is covered. $C_{P\mathrm{rms}}$ in the tunnel was 0.20% (Ref. 9), which is much lower than the value of 2.0% in the typical blowdown tunnel of 2.56 × 1.83 m, ONERA-S3 (Ref. 10); its test section is 1.93 m wide and 1.75 m high.

Test Models

A 23.3% scale model of an experimental airplane (Fig. 2), which has a planform of 1.87 m length and 1.1 m span width, was used in S2MA. The model has 37 ports at 30, 50, and 70% semispanwise stations of the port wing; it has 28- and 40-element hot-film sensors mounted flush with the starboard wing surface at 30 and 70% semispanwise stations, respectively. In addition, the starboard wing section, located from 0 to 60% chordwise and from 12.8 to 75.5% semispanwise stations, is made of resin to enable measurement of the surface temperature distribution using an infrared camera.

Because the test section of the FHI tunnel is much smaller than that of S2MA, we used two 15.7% scale half-models (Fig. 3) in the FHI tunnel to realize test Reynolds numbers within the range of those in S2MA. The two half-models, one for pressure measurement and the other for transition, have identical configurations of 1.139 m length and 0.37 m span width. The pressure model has 40 static pressure ports at 30, 50, and 70% semispanwise stations. The transition model (Fig. 3) has 28- and 32-element hot-film sensors at 30 and 70% semispanwise stations, respectively.

Well-known disadvantages of half-model testing are the mounting effect and the increased wall interference.[11] Accordingly, we set the half-models 34 mm from the wall with a support, as shown in Fig. 3, to exclude the influence of the tunnel wall boundary layer. A sharp-edged reflector plate was set between the model and the support. As a result, shock waves generated at the support and the leading edge of the reflector plate were confined to between the plate and the wall and had no influence on the model.[12] Furthermore, we eliminated the influence of a very thin boundary layer developing in the 39-mm gap between the tip of the plate and the nose of the model by setting the model 1 mm from the plate.

The inconsistency between transition data in different tunnels is attributed to different freestream turbulence levels and surface roughnesses of models. Thus, total pressure fluctuation was measured in the tunnels using unsteady pressure transducers. Also, the arithmetic average roughness amplitudes of both models are set below 0.2 μm, which is lower than the 0.25 μm of a well-known transition model, the Arnold Engineering Development Center 10-deg cone.[13]

Fig. 2 Model, 26.6% scale.

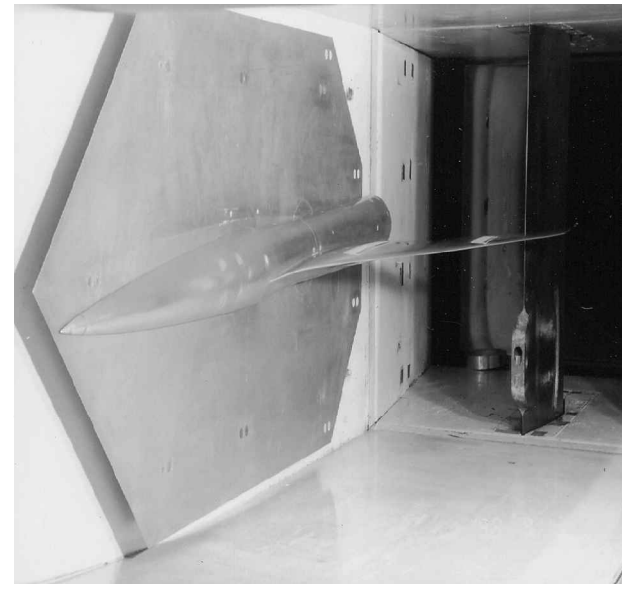

Fig. 3 Half-model, 15.7% scale, for transition measurement.

Data Processing

Definition of Transition Location

Consistent definitions of the transition point are required because there is considerable scatter in transition data due to the different methods used for transition measurement.[14,15] At supersonic speeds, an analysis of a large body of heat transfer data by Bertram and Neal[16] has shown that the choice of the virtual origin at the point of maximum surface temperature gives the most consistent results. Accordingly, the location of the maximum surface temperature

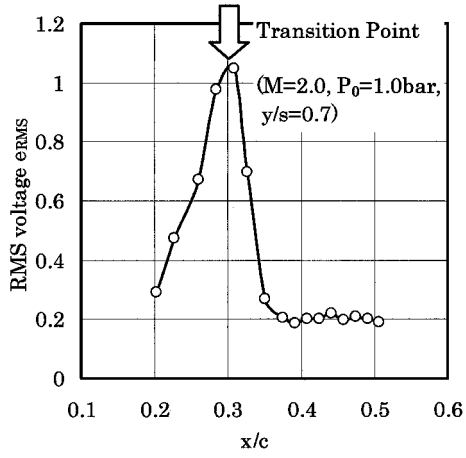

Fig. 4 Examples of hot-film voltage fluctuation along the wing chord and transition point.

is defined as the transition point in the present research. It is established by Owen[15] that the location of peak voltage fluctuation determined using hot-film sensors on surface coincides with the maximum burst frequency location and the maximum surface temperature location.[17] Hence, the location of peak voltage fluctuation is also defined as the transition point in the present research. Examples of the hot-film rms voltage and transition point are given in Fig. 4; an arrow indicates the transition point.

In the comparison of the transition locations identified using different sensors, the accuracy of the measurement must be considered. The accuracy of the transition Reynolds number obtained using the infrared camera is estimated to be 2%. The estimation is based on the image length of 1.0 mm corresponding to one pixel and temperature resolution of 0.5°C. The accuracy of the transition Reynolds number determined using hot-film sensors is estimated to be 3%, which is based on the spacing of sensors, 2.54 mm, and an assumed estimation error of 2% in the process of defining the location of the peak voltage fluctuation.

Freestream Turbulence

When total pressure is measured in supersonic flow, a normal shock wave exists upstream of the probe; consequently, total pressure measured at the tip of the probe is equal to the total pressure P_{02} downstream of the shock, that is, the pitot pressure. Thus, the total pressure fluctuation measured using an unsteady pressure transducer at the stagnation point is the pitot pressure fluctuation P'_{02}. Hence, total pressure fluctuation is defined as the rms average of pitot pressure fluctuation P'_{02}, divided by pitot pressure in the present research, as in previous research.[5,13]

Total pressure fluctuation is measured with bandwidth from 25 Hz to 20 kHz in the FHI tunnel, and from 125 Hz to 100 kHz in S2MA. All of the pressure transducers are 1.6 mm in diameter.

Results and Discussion

Pressure Distribution on the NLF Wing

Before the transition measurements, we compared pressure distributions for the two models with computational fluid dynamics (CFD) results obtained with the three-dimensional Navier–Stokes code. This code uses the Baldwin–Lomax model and was previously validated by experiments and other numerical codes.[18] Comparisons between the measured and calculated pressure distributions at 30 and 70% semispanwise stations are shown in Figs. 5 and 6, respectively. The measured results at $\alpha = 1.73$ deg agree well with the CFD results calculated at the design angle of attack of 2 deg. The discrepancy of 0.27 deg can be explained by a change in the local angle of attack caused by either 1) bending of the wing or 2) change in downwash distribution on the wing due to the existence of the large model in the tunnel. We measured the transition at $\alpha = 1.73$ deg because the present research is aimed at validating

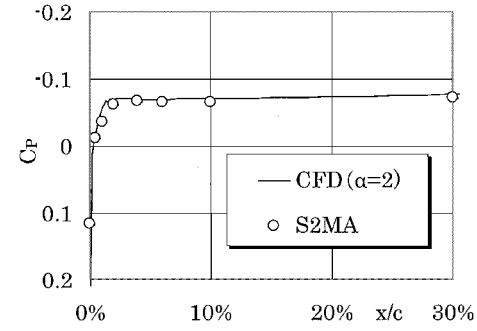

Fig. 5 Comparison between the measured and calculated pressure distribution at 30% semispanwise station ($M = 2$ and $\alpha = 1.73$ deg, in S2MA).

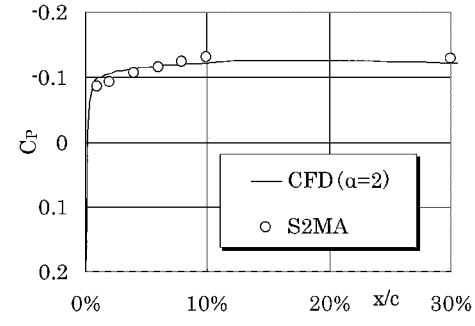

Fig. 6 Comparison between the measured and calculated pressure distribution at 70% semispanwise station ($M = 2$ and $\alpha = 1.73$ deg, in S2MA).

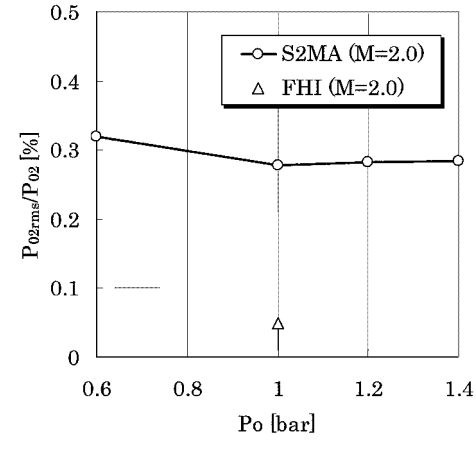

Fig. 7 Pitot pressure fluctuation in the FHI tunnel and S2MA.

the NLF effect of the designed pressure distribution. The models exhibited pressure distributions close to the designed ones; thus, it is confirmed that we can validate the NLF effect using these models.

Freestream Turbulence Level in Wind Tunnels

We measured pitot pressure fluctuation in the tunnels to determine their freestream turbulence levels. Figure 7 shows the pitot pressure fluctuation plotted against total pressure at $M = 2$. It is clear that the total pressure has little effect on pitot pressure fluctuation, that is, the freestream turbulence level in S2MA, so that by varying the total pressure in S2MA, the unit Reynolds number effect on transition can be studied. The average pitot pressure fluctuation at $M = 2$ was 0.29% in S2MA and a very low value of 0.05% in the FHI tunnel. This value lies within the range of the pitot pressure fluctuation at $M = 2$ in flight, which is from 0.02 to 0.06% (Ref. 10).

Transition Location on the NLF Wing

Figure 8a shows a surface temperature distribution of the area shown in Fig. 8b, determined using the infrared camera. Distortion and aeroelastic deformation are corrected by three-dimensional affine transformation in Fig. 8. The color changes from black to white with increasing temperature. The transition line is shown by a line and corresponds to the location of maximum surface temperature. There is no rapid change of the transition point in the spanwise direction. Consequently, transition characteristics at 30 and 70% semispanwise stations represent those of the inner and outer parts of the wing, respectively.

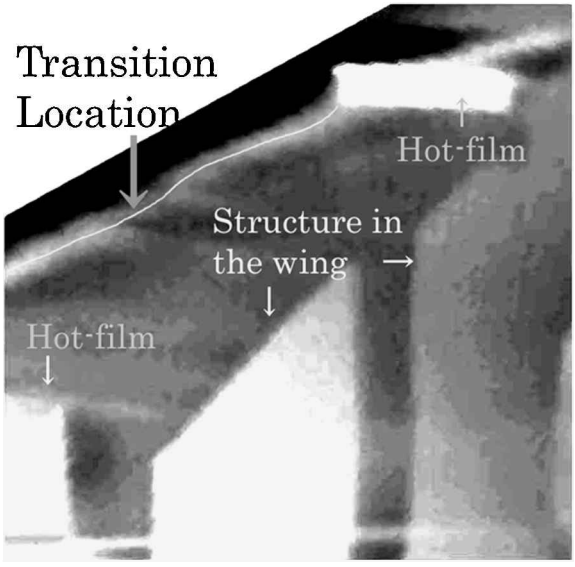

Fig. 8a Surface temperature distribution determined using infrared camera (M = 2, α = 2 deg and P_0 = 1.0 bar).

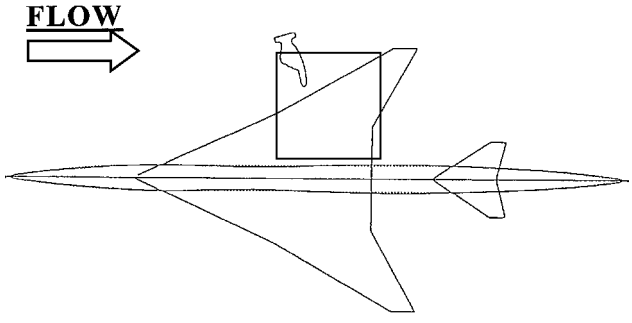

Fig. 8b Area of the surface temperature distribution.

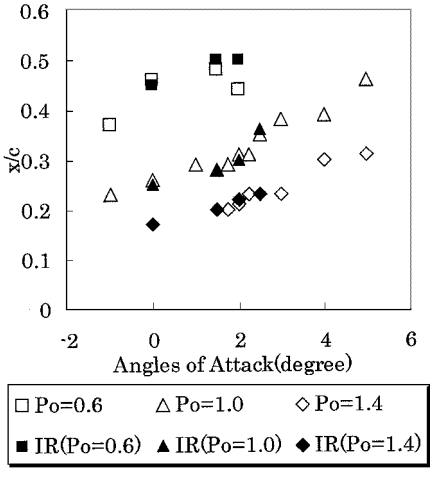

Fig. 9 Effect of total pressure on the transition location at 70% semispanwise station at M = 2.

Figure 9 shows the effect of total pressure on the transition location at the 70% semispanwise station measured using hot-film sensors and the infrared camera. The transition locations move forward as total pressure increases. Transition locations identified using the infrared camera agree well with those obtained using hot-film sensors. This confirms Owen's report[15] and proves the consistency of the present definition of the transition points.

The results shown in Fig. 9 are replotted as transition Reynolds numbers in Fig. 10. All of the data fall above a single curve. The transition Reynolds numbers at the 30% semispanwise station are shown in Fig. 11. Again, all of the data fall above a single curve. This is noteworthy because it shows that there is no unit Reynolds number effect on the transition Reynolds number of the NLF wing; this is quite similar to results for flat plates and sharp cones. The reason for this similarity can be sought in the very flat pressure distributions of the NLF wing, as in the cases of flat plates and sharp cones.

It is clear from Fig. 11 that the longest laminar region at the 30% semispanwise station is achieved at $\alpha = 1.73$ deg, where the design pressure distribution is realized. Even a slight deviation in the angle of attack from 1.73 deg moves the transition location significantly upstream. This confirms the NLF effect of the designed pressure distribution on the inner part of the wing. Pressure distributions at the 30% semispanwise station are shown in Fig. 12. Figure 12 shows that the narrowest accelerating region at the 30% semispanwise station

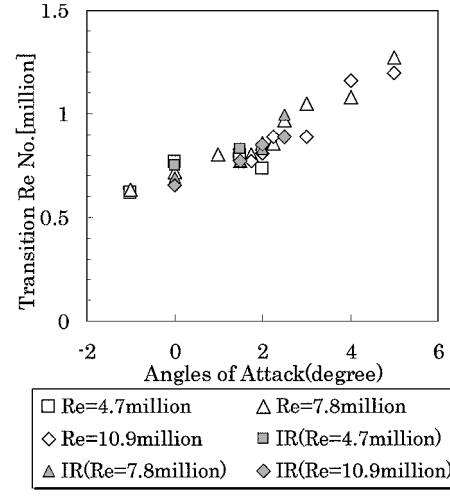

Fig. 10 Effect of angle of attack on transition Reynolds numbers at 70% semispanwise station at M = 2.

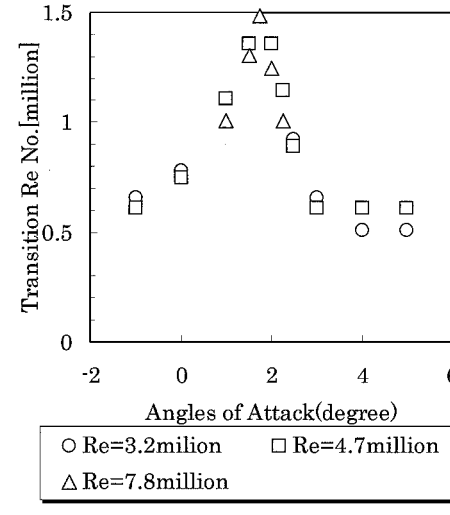

Fig. 11 Effect of angle of attack on transition Reynolds numbers at 30% semispanwise station at M = 2.

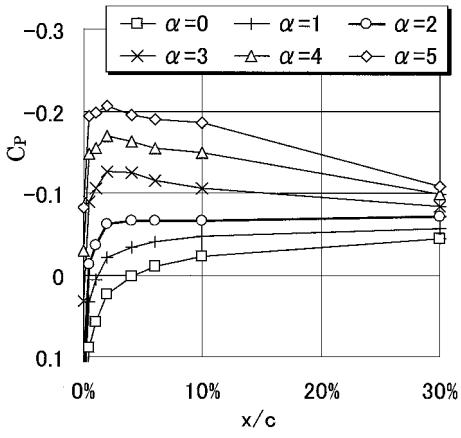

Fig. 12 Pressure distributions at 30% semispanwise station at $M = 2$.

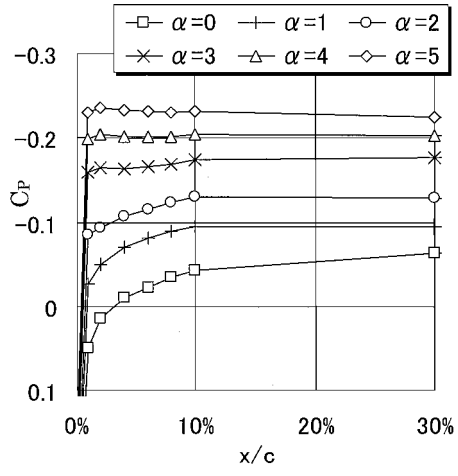

Fig. 13 Pressure distributions at 70% semispanwise station at $M = 2$.

is realized at $\alpha = 1.73$ deg, which minimizes the development of crossflow velocity components that amplify crossflow instability. Figure 12 also shows that the pressure distribution at $\alpha = 0$ deg has a gradual pressure gradient near the leading edge, which is quite similar to that in the case of conventional supersonic aircraft.

On the other hand, Fig. 10 shows that the longest laminar region at the 70% semispanwise station is achieved at $\alpha = 5$ deg, which is far from the design angle of attack of 2 deg. Pressure distributions at the 70% semispanwise station are shown in Fig. 13. It is clear from Fig. 13 that pressure distribution at $\alpha = 5$ deg has a narrower accelerating region than that at $\alpha = 2$ deg; this reduces the development of crossflow velocity components. Figure 13 also shows that the pressure distribution at $\alpha = 0$ deg has a gradual pressure gradient near the leading edge, which is quite similar to conventional supersonic aircraft. The transition location moves rearward with increasing angle of attack from 0 deg. This confirms the NLF effect of the pressure distribution on the outer part of the wing, similar to the inner part.

Numerical Analysis of the Transition

The principle behind laminar flow control is to keep the growth of disturbances within acceptable limits so that three-dimensional and nonlinear effects do not cause a breakdown to turbulence. With this philosophy, one only deals with linear disturbances, and, hence, the difficulties in transition prediction do not directly arise.[19] We analyzed the transition characteristics of the NLF wing using a linear stability analysis code based on the three-dimensional compressible linear stability theory and the e^N method with an envelope method strategy. Compressible laminar boundary-layer profiles were calculated using methods developed by Kaups and Cebeci.[20] N is defined as an integration of amplification rates of small disturbances with several frequencies. N was integrated along a polar arc normal to the leading edge in the code because the Kaups and Cebeci method was formulated in a polar coordinate system.[20] Nonparallel and curvature effects are not included in the present code. The code is validated experimentally and using another linear stability code developed by Arnal et al. based on the envelope method.[21] The chordwise distribution of the N values and propagation directions of disturbances on a 10-deg cone and the NLF wing obtained using the two codes agreed very well.[21]

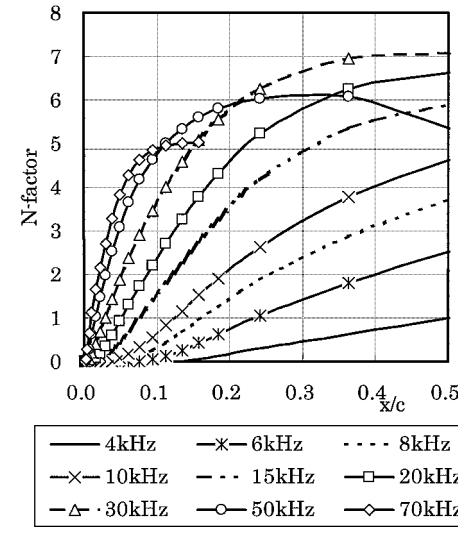

Fig. 14 Typical stability analysis result at 70% semispanwise station at $M = 2$ ($\alpha = 2$ deg and $P_0 = 1.4$ bar).

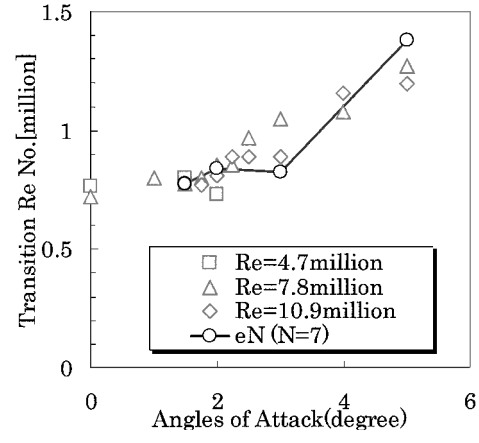

Fig. 15 Summarized stability analysis results at 70% semispanwise station ($M = 2$ and $P_0 = 1.0$ bar).

Figure 14 shows a typical stability analysis result at the 70% semispanwise station at $M = 2$; the coordinates correspond to the envelope of N values. The crossflow and streamwise instabilities are not distinguished here; the growth of disturbances of different frequencies is computed for whichever propagation angle of disturbance that gives the maximum growth rate. According to a transition measurement on a 10-deg cone in S2MA,[9] $N = 7$ corresponds to the end of the transition at $M = 2$ in the tunnel. Figure 14 indicates that the end of the transition is located at the 36% chordwise station when $N = 7$. Figure 15 summarizes the measured transition location and that calculated by the same approach in the range of angle of attack from 1.5 to 5 deg, where the existence of the NLF effect is inferred from the shape of the pressure distribution in Fig. 13. It is clear from Fig. 15 that the calculated locations agree with the measured locations quantitatively. This implies that the present analysis results reproduce the real transition on the NLF wing satisfactorily.

Figure 16 shows the chordwise distribution of the propagation direction of the disturbance calculated using the present code under the same conditions as in the case of Fig. 15. Here, Ψ is defined as the

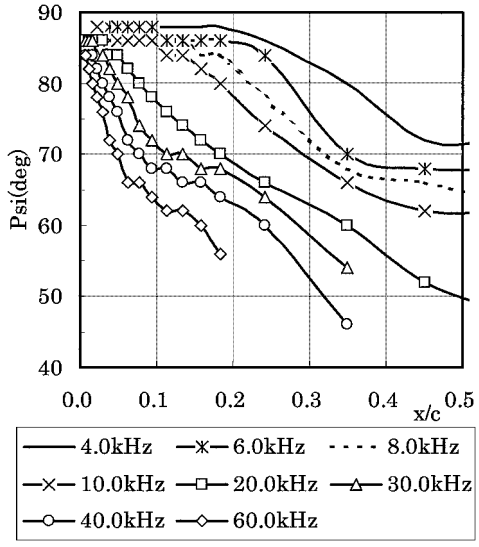

Fig. 16 Chordwise distribution of propagation direction of the disturbance at 70% chordwise station (M = 2 and P_0 = 1.4 bar).

angle between the propagation direction and the outer streamline. According to the compressible linear stability theory, the most unstable direction Ψ_{max} of streamwise disturbances ranges from 40 to 70 deg, and Ψ_{max} of crossflow disturbances lies in a narrow range between 85 and 89 deg (Ref. 5). Figure 16 shows that Ψ_{max} of the wave with the maximum amplified frequency is 86 deg near the leading edge, which indicates that crossflow instabilities are dominant. On the other hand, Ψ_{max} ranges from 55 to 60 deg near the transition point of the 36% chordwise station, which indicates that streamwise instabilities are dominant. Furthermore, the unit Reynolds number's independence of the transition Reynolds numbers is quite similar to that of flows on flat plates and sharp cones that are dominated by streamwise instabilities. Such evidence suggests that the transition on the NLF wing is dominated by streamwise instabilities.

However, further measurement or analysis, such as a study by Haynes and Reed,[22] is needed for justification of the dominance of streamwise instabilities because the envelope method lacks physical information on the transition process; this is because streamwise and crossflow instabilities will exert additive effects in the method, and it is assumed that a crossflow wave can suddenly change to a streamwise wave within a very short distance.[3] In addition, the unit Reynolds number's independence of the results may reflect velocity fluctuations, the spectral content of the pressure fluctuations, and other factors.

Consideration of Surface Roughness

Before we predict the transition location of the NLF wing in flight, we must consider the influence of surface roughness on the transition. Some experiments investigating the influence of surface roughness were conducted in the FHI tunnel because of its low freestream turbulence level. Roughness was applied to the 70% semispanwise station where the designed pressure distribution was realized.

The concept of a critical roughness Reynolds number is adopted here because the concept fits numerous experimental data, although it has no physical support.[23,24] The critical roughness Reynolds number is evaluated based on conditions at the roughness height[21]:

$$Re_{kk} = \rho_k U_k h / \mu_w \tag{1}$$

In the case of distributed roughness, h in the preceding expression is replaced by k.

The average roughness height is 0.2 μm on the model, which is nearly the limit of model production capability. We used it as a clean base configuration and applied isolated and distributed roughness with different heights to the wing. Cylindrical isolated roughness elements were obtained by applying rub-on symbols from transfer sheets commonly used in graphic arts. This is the same method as that described in Ref. 25. The distributed roughness was obtained by applying different paints or sand grains with different radii. Average and maximum roughness heights were directly measured using a profilometer after each experiment to check for nonuniform roughness height distribution.

Figure 17 shows the roughness height effect on transition Reynolds number. Open symbols correspond to isolated roughness at different chordwise stations; they fall above a single curve. This shows that the effect of isolated roughness height on transition did not change with roughness location. The reason for this can be sought in the nearly zero pressure gradient downstream of the 2% chordwise station.

Filled symbols in Fig. 17 correspond to the distributed roughness; a dotted quadratic curve is drawn, similar to the solid curve for the isolated roughness, because there are only four points of distributed roughness data. The roughness Reynolds numbers for the distributed roughness case are computed at 6% chordwise station, which is the average chordwise location of the distributed roughness. Figure 17 shows that distributed roughness with an average height of more than 10% of the boundary-layer thickness has an effect on transition location. This corresponds to the critical roughness Reynolds number of 140 and the roughness height of 6 μm in flight. The average roughness height of a real experimental airplane is 1.0 μm. The surface will be further polished immediately before the flight to realize the average roughness height of 0.3 μm. The result indicates that surface roughness on the NLF wing negligibly affects the transition on the wing in flight.

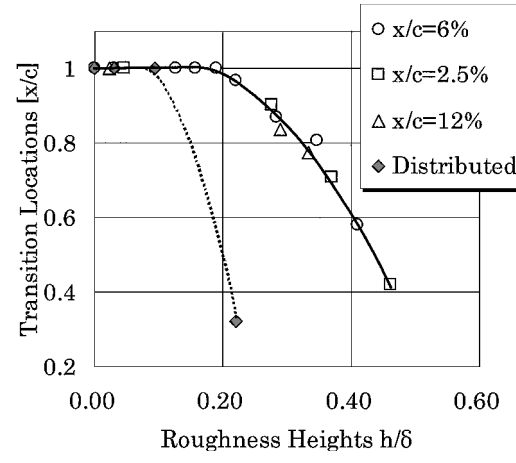

Fig. 17 Roughness height effects on transition Reynolds number at 70% semispanwise station at M = 2.

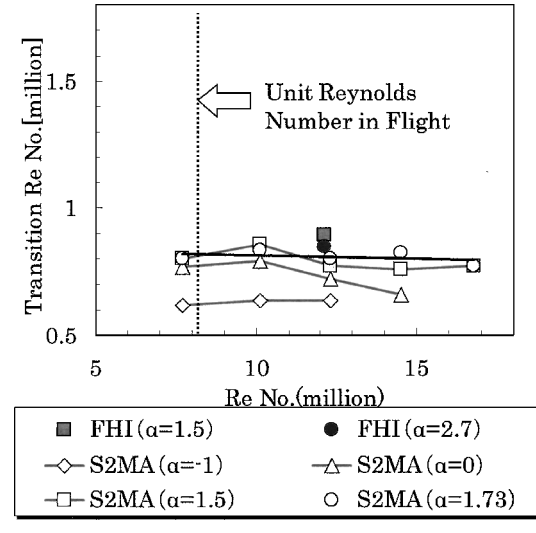

Fig. 18 Unit Reynolds number effect on transition Reynolds numbers at 70% semispanwise station at M = 2.

Prediction of Transition Location in Flight

Figure 18 shows the unit Reynolds number effect on transition Reynolds numbers at the 70% semispanwise station. Open symbols correspond to the values in S2MA. Note that the transition Reynolds numbers in S2MA are constant for any unit Reynolds numbers. Filled symbols correspond to the values in the FHI tunnel of low turbulence level, comparable to an in-flight environment; they fall slightly above the S2MA test results. This indicates that the freestream turbulence has little effect on the transition on the NLF wing. The independence of the results of the unit Reynolds numbers implies that the transition Reynolds number at the design angle of attack of 2 deg is estimated to be 8×10^5 in flight, and the transition point is estimated to be at the 9% chordwise station. It is, however, debatable whether or not the freestream turbulence has an effect on the transition on the NLF wing because the pressure fluctuation may be larger than the present value in the FHI tunnel, which was measured without the presence of a large reflection plate.

Conclusions

Transition on a supersonic natural laminar flow wing with a sweepback angle of more than 60 deg was measured using hot-film sensors and an infrared camera at Mach 2 in two supersonic wind tunnels. The NLF effect of the wing was confirmed. We also showed that the unit Reynolds number had no effect on the transition Reynolds numbers of either the inner or outer part of the NLF wing; the transition Reynolds number was 8×10^5 in the outer part of the wing at Mach 2. According to the independence of the results of the unit Reynolds number, the transition location was estimated to be at the 9% chordwise station, but there is room for further investigation.

Acknowledgments

The authors wish to acknowledge the help and advice received from Daniel Arnal of ONERA, with whom we are currently conducting joint research on the supersonic boundary-layer transition. We also wish to thank Yoshine Ueda, for providing linear stability analysis results and Kenichiro Suzuki for correction of infrared images by three-dimensional affine transformation. Both are supporting staff members of primary research at the National Aerospace Laboratory, Japan.

References

[1]Yoshida, K., "Overview of NAL's Program Including the Aerodynamic Design of the Scaled Supersonic Experimental Airplane," von Kármán Inst. Special Course "Fluid Dynamics Research on Supersonic Aircraft," RTO-EN-4, No. 15, 1998.

[2]Wagner, R. D., Maddalon, D. V., Bartlett, D. W., and Collier, F. S., Jr., "Fifty Years of Laminar Flow Flight Testing," Society of Automotive Engineers, Paper SAE 881393, 1988.

[3]Arnal, D., "Boundary Layer Transition: Prediction, Application to Drag Reduction," Rept. 793, AGARD, 1993, p. 5.

[4]Joslin, R. D., "Aircraft Laminar Flow Control," *Annual Review of Fluid Mechanics*, Vol. 30, 1998, pp. 1–30.

[5]Dougherty, N. S., Jr., and Fischer, D. F., "Boundary-Layer Transition on a 10-deg Cone: Wind Tunnel/Flight Correlation," AIAA Paper 80-0154, 1980.

[6]Beckwith, I. E., "Development of a High Reynolds Number Quiet Tunnel for Transition Research," *AIAA Journal*, Vol. 13, No. 3, 1975, p. 300.

[7]Pope, A., and Goin, K. L., *High-Speed Wind Tunnel Testing*, Wiley, New York, 1965, p. 5.

[8]Koshioka, Y., and Shiozawa, N., "Freestream Turbulence Measurement Results in Fuji Heavy Industries Ltd. High-Speed Wind Tunnel," *Proceedings, 46th Wind Tunnel Conference*, Fuji Heavy Industries Ltd., Utsunomiya, Japan, 1996 (in Japanese).

[9]Fontaine, J., Arnal, D., and Juillen, J. C., "Qualification de la Veine Supersonique de S2MA avec le Cone Pression 10° en Ureol du CEAT," P. V. d'Essais ONERA 6/1721 DY, 1993.

[10]Dougherty, N. S., Jr., "Influence of Wind Tunnel Noise on the Location of Boundary-Layer Transition on a Slender Cone at Mach Numbers from 0.2 to 5.5," Arnold Engineering Development Center, Tennessee, AEDC-TR-78-44, Vol. 1, 1980.

[11]Boersen, S. J., and Elsenaar, A., "Half-Model Testing in the NLR High Speed Wind Tunnel HST: Its Technique and Application," CP-348, AGARD, 1984, p. 23.

[12]Yoshida, K., Ishida, Y., Noguchi, M., Ogoshi, H., and Inagaki, K., "Experimental and Numerical Analysis of Laminar Flow Control at Mach 1.4," AIAA Paper 99-3655.

[13]Fisher, D. F., Dougherty, N. S., Jr., "In-Flight Transition Measurement on a 10 degree Cone at Mach Numbers from 0.5 to 2.0," NASA TP-1971, 1982.

[14]Pate, S. R., and Schueler, C. J., "An Investigation of Radiated Aerodynamic Noise Effects on Boundary-Layer Transition in Supersonic and Hypersonic Wind Tunnels," AIAA Paper 68-375, 1968.

[15]Owen, F. K., "Transition Experiments on a Flat Plate at Subsonic and Supersonic Speeds," *AIAA Journal*, Vol. 8, No. 3, 1970, pp. 518–523.

[16]Bertram, M. H., and Neal, L., Jr., "Recent Experiments in Hypersonic Boundary Layers," NASA TM X-56335, 1965.

[17]Arnal, D., "Boundary Layer Transition: Predictions Based on Linear Theory," Rept. 793, AGARD, 1993, p. 30.

[18]Takaki, R., Iwamiya, T., and Aoki, A., "CFD Analysis Applied to the Supersonic Research Airplane," *Proceedings of the 1st International CFD Workshop for Supersonic Transport Design*, National Aerospace Lab., Tokyo, 1998, pp. 68–72.

[19]Saric, W. S., "Laminar-Turbulent Transition: Fundamentals," Rept. 793, AGARD, 1993, p. 4.

[20]Kaups, K., and Cebeci, T., "Compressible Laminar Boundary Layers with Suction on Swept and Tapered Wings," *Journal of Aircraft*, Vol. 14, No. 7, 1977, pp. 661–667.

[21]Yoshida, K., Ueda, Y., Sugiura, H., Tokugawa, N., Atobe, T., Arnal, D., Archamboud, J. P., and Seraudie, A., "Boundary Layer Transition Analysis on NEXST-1 Airplane: NAL-ONERA Cooperative Research Project," *Proceedings of the International Workshop on Supersonic Civil Aircraft*, National Aerospace Lab., Tokyo, 2001, p. 1.

[22]Haynes, T. S., and Reed, H. L., "Simulation of Swept-Wing Vortices Using Nonlinear Parabolized Stability Equations," *Journal of Fluid Mechanics*, Vol. 405, 2000, pp. 325–349.

[23]Reda, D. C., "Roughness-Dominated Transition on Nosetips, Attachment Lines, and Lifting-Entry Vehicles," AIAA Paper 2001-0205, 2001.

[24]Bradshaw, P., "A Note on 'Critical Roughness Height' and 'Transitional Roughness,'" *Physics of Fluids*, Vol. 12, No. 6, 2000, pp. 1611–1614.

[25]Radeztsky, R. H., Reibert, M. S., and Saric, W. S., "Effect of Isolated Micron-Sized Roughness on Transition in Swept-Wing Flows," *AIAA Journal*, Vol. 37, No. 11, 1999, p. 1372.